PROBABILISTIC APPROACH FOR CORRECTION OF FIVE HOLE PROBES: EFFECT OF MACH AND WALL INTERACTION

Lakshya Bhatnagar, Andrea Ruan, Guillermo Paniagua
Purdue University, West Lafayette, IN, USA

ABSTRACT

Five-Hole directional probes are commonly used in experimental fluid mechanics to assess flow angles, total and static pressure. Five-hole probes undergo a calibration procedure to relate these quantities to the pressure readings. However, the pressure-flow angle relationship may change due to the flow distortion induced by the probe; such distortion varies with Mach and Reynold's numbers. This manuscript analyzes the probe–test section effects. A correction methodology is developed by analyzing the variation of the pressure change due to these effects. A Gaussian regression model is developed to reduce the number of CFD simulations required for the range of the calibrated angle. This is used to provide enough data to generate a correction model. This methodology is then applied to an experimental calibration map to correct data taken at a Mach number of 0.6 with a calibration performed at Mach 0.2.

NOMENCLATURE

α	Yaw angle
β	Pitch angle
C_p	Pressure Coefficient
d	Diameter of the probe head
l	Length of the probe head
M	Mach number
$\dot{m}$	Massflow
P	Pressure
P_0	Total Pressure

ABBREVIATIONS

CFD	Computational Fluid Dynamics
GP	Gaussian Process

1. INTRODUCTION

Directional probes allow the measurement of flow angles (yaw and pitch) and total and static pressure using a single probe. They must be calibrated to relate their raw measurements to these derived quantities. However, the calibration process does not consider the effect of probe blockage and the difference in experimental to calibration conditions that change the mapping of the raw measurement to derived quantities. This is important because the calibration is not done in the same flow condition the probes see in the experiment. Gaetani and Persico [1] showed a variation of their calibration coefficients for the exact value of yaw angle for different Mach numbers. Smout and Ivey [2], [3] showed that the proximity to a wall changed the flow field around a probe, and this effect needs to be considered during calibration. The implication is that probes must be calibrated in the same duct and at the same operating condition that they will see during a test. This is not always feasible; corrections are required for the measured data. Numerical simulations allow us to replicate flow behavior in the experimental test section. This was demonstrated by Argüelles Díaz et al. [4], who used numerical simulations to build a model for a three-hole trapezoidal probe. Simulations also allow for new calibration mappings, such as the zonal calibration by Delhaye et al. [5]. This manuscript presents a method to leverage numerical data into a simple model for correcting these effects.

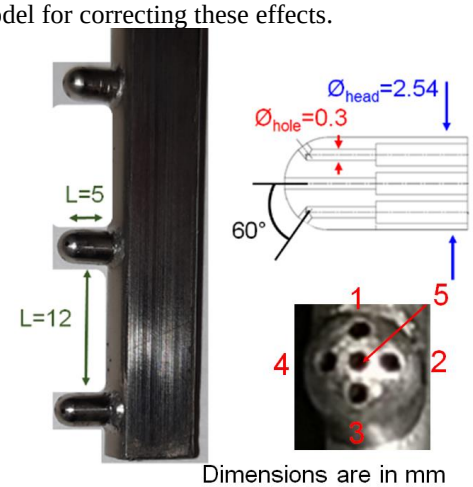

Figure 1Five-hole probe for angle measurement, showing head length and space between heads, internal schematic, and nomenclature used for the holes.

In the test rig, both the measurement probes and the flow path geometry affect the flow field. This was evident in the change in the pressure profile of a test vane when the measurement probes were inserted behind the vanes [6]. At the same time, it is observed that the test rig geometry also affects the reading of the measurement probe. For the test case described in [6], a three-head five-hole probe

was used, as shown in Figure 1. The heads are hemispherical, with holes located at 60 degrees relative to the axis. The heads per rake were selected to minimize the probe blockage while providing adequate space for 0.305 mm inner diameter pressure lines.

This blockage effect is exacerbated in a transonic flow in the vicinity of the endwall, leading to an artificial pitch angle indication in the flow measurement. To better understand this flow distortion, a series of RANS simulations were performed with the numerical domain shown in Figure 2a) ; this was documented in [6]. A whole five-hole probe geometry adjacent to the shroud is simulated in a passage downstream of the vane at two radial locations, near the wind-tunnel shroud and mid-span. Figure 2b), shows the top head at two different radial locations and highlights the effect of the combined blockage of the probe stem and the shroud that leads to a local acceleration region near the top of the probe head where the measurement holes are located, not seen at a radial location away from the shroud. The probe measures this as a decrease in pressure for the affected hole, distorting the final angle calculation.

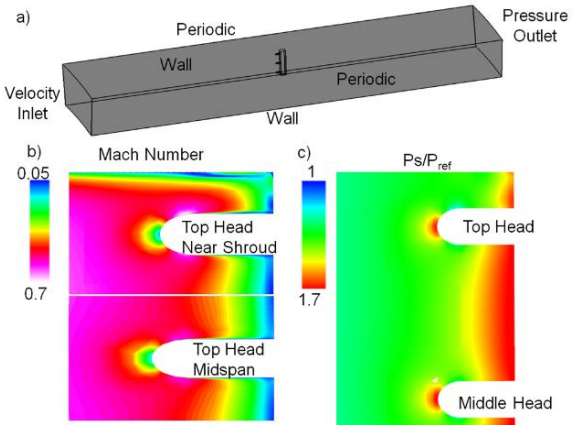

Figure 2 a) Computational domain of the probe, b) Mach number contour in front of the probe highlighting local acceleration in the near shroud compared to the mid-span location c) Pressure distortion at pitch holes.

We see that the probe endwall interaction results in a distortion in the local Mach number around the measurement holes, which leads to a different pressure reading. This also implies that the probe heads will read different pressure values for a given flow angle at various Mach numbers. This paper presents a methodology to correct this effect using CFD data.

2. CALIBRATION MAP APPROACH

The approach used to convert pressure reading of the holes to derived quantities (flow angles, total and static pressure) is the coefficient map approach which has been described extensively in literature by works such as Treaster and Yocum [7], Pisasale and Ahmed [8] and Yasa and Paniagua [9]. This method converts the pressure from each hole, taken at different flow conditions, into a map of coefficients. Equation (1) shows the coefficient that is primarily dependent on the yaw angle

$$Cp_v = \frac{P_2 - P_4}{P_5 - P_{avg}} \tag{1}$$

where, P_2, P_4, P_5, are pressures at holes 2,4 and 5, shown in Figure 1. P_{avg} is the average of all the holes except the center one, given as

$$P_{avg} = mean(P_1, P_2, P_3, P_4). \tag{2}$$

Equation (3) shows the coefficient that is primarily dependent on the pitch angle

$$Cp_w = \frac{P_1 - P_3}{P_5 - P_{avg}} \tag{3}$$

where, P_1, P_3 are pressures at holes 1 and 3.

The total pressure and static pressure are related by two coefficients given by Equation (4)

$$Cp_0 = \frac{P_5 - P_s}{P_0 - P_s} \tag{4}$$

and Equation (5)

$$Cp_{avg} = \frac{P_{avg} - P_s}{P_0 - P_s} \tag{5}$$

where, P_0 is the flow total pressure and P_s is the flow static pressure.

The relationship between C_{pv} and C_{pw} is shown in Figure 3a) for one head of the probe. Figure 3b) and c) show the variation of C_{p0} and C_{pavg} respectively with C_{pv} and C_{pw}. As it can be seen, the pressure readings differ from the total pressure and static pressure readings more as we go to higher yaw (higher C_{pv}) or pitch (higher C_{pw}). The maximum is not centered at zero due to manufacturing errors highlighting the importance of experimental calibration.

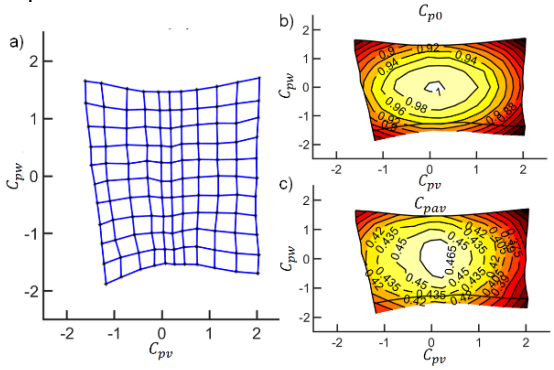

Figure 3 a) Calibration map of C_{pw} vs. C_{pv} b) Calibration map of C_{p0} against yaw and pitch angles, c) Calibration map of C_{pavg} against yaw and pitch angles

This method is simple to implement and validate. The coefficients used, however, are sensitive to Mach and Reynold's number. Therefore, it is advised to calibrate the probes at the expected flow conditions of the test. The literature tackles this by making multiple calibration maps at different Mach and Reynold's numbers. However, this isn't always feasible, and interpolation is still needed between the Mach numbers at which the maps are available.

3. MACH AND ENDWALL EFFECTS

To better understand the effect of Mach number and the proximity of the probe to the endwalls, a numerical analysis through Reynolds Averaged Navier-Stokes (RANS) simulations, was carried out for the directional probe at two different Mach numbers, seven yaw angles, and two different radial locations. To assess if the impact can be reduced by increasing the distance of the measurement head from the probe body, the same conditions were run for another geometry with a length-to-head diameter ratio (l/d) of 10. This value is taken from design recommendations from Sieverding [10] for transonic flows.

The fluid domain is shown in Figure 4 a). The channel height and radial location of the probes are taken from the test case, and the actual radial locations of the probe are described in Bhatnagar et al.[6].

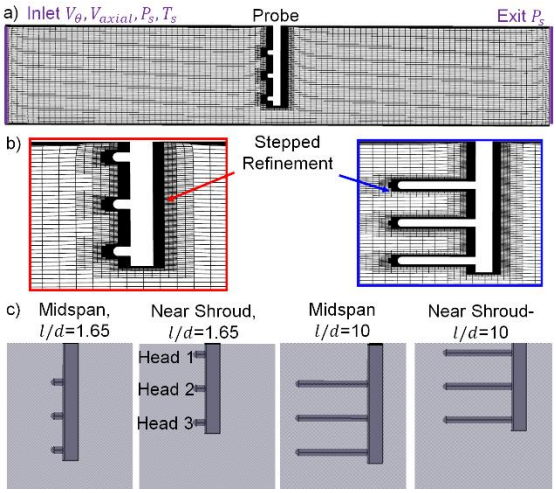

Figure 4 a) Fluid domain showing inlet, exit planes and probe location, b) stepped mesh refinements for both l/d=1.65 (left) and l/d=10 (right) case, c) the two radial locations Mid-span and Near Shroud for both l/d=1.65 and l/d=10 cases.

The flow angles are set at the inlet by imposing the tangential and axial velocities. It is assumed that there is no radial flow at the inlet. The total velocity magnitude is used to define the inlet Mach number. An initial guess of static pressure and temperature is imposed at the inlet, which changes with each iteration. At the exit, static pressure is set. The simulations are carried out in Ansys Fluent, with a K-omega SST turbulence model, with the experimentally measured turbulence intensity level of 6% imposed at the inlet. Gas density is assumed to behave like an ideal gas, and viscosity is calculated from the Sutherland law.

The mesh for one radial location for l/d=10 and l/d=1.65 each is shown in Figure 4 b). The mesh is unstructured and generated in Numeca Hexpress. The figure shows that the fluid domain is kept the same size, with refinements near the probe geometry. Three levels of refinements are carried out from the freestream to the probe surface. A viscous layer is inserted at each solid surface with an initial layer thickness of 1μm

The two radial locations denoted as Mid-span, where Head 2 is at mid-span, and Near Shroud, where Head 1 is closest to the top endwall, are used for each l/d ratio probe, as shown in Figure 4 c). Three meshes were generated to assess the grid dependency of the results. The initial number of cells is changed, but the ratio for the refinement and the first layer thickness of the viscous layer is kept constant for each mesh.

Figure 5 shows the results from the different meshes for the l/d=1.65 case at the near shroud radial location.

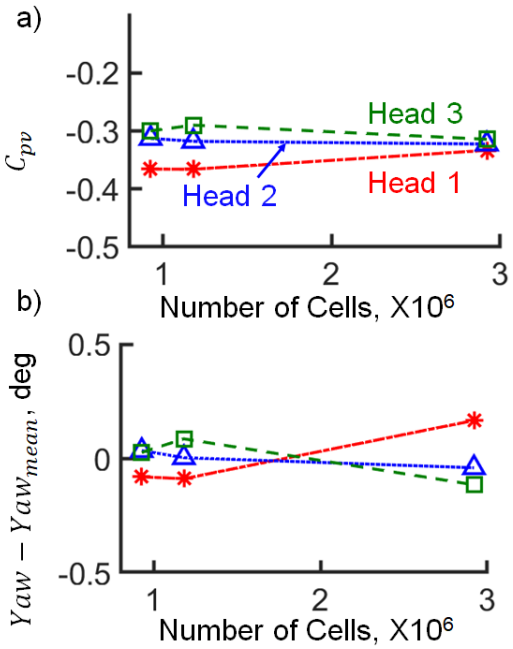

Figure 5 a) Variation of C_{pv} for each head for three difference meshes for l/d=1.65 at Near Shroud location shows variation within 5%, b) calculated yaw angle from the C_{pv} value shows variation less than 0.2 degrees.

Figure 5a) shows the variation of C_{pv}value, from Equation (1), for each head for the three meshes used. It is seen that the maximum difference between the values is less than 0.1. To assess the impact of this variation on yaw angle, a calibration

map is used from a five-hole probe of l/d =1.65 and the numerical C_{pv} are used to extract the flow angle. The Mach number of both these simulations and the experimental calibration is 0.15. The calibration map is not directly applicable to the result of the simulations since the numerical probe holes are perfectly symmetric and the actual probes are not due to manufacturing errors. However, it allows us to get an angle estimate from the obtained C_{pv}values, shown in Figure 5b). The variation in the angles is less than 0.15 degrees from the mean. Due to the small variation with mesh refinement, the mesh of 1.2 million cells is selected.

Figure 6 a), b), and c) show the Mach contour and streamlines around the head for l/d =1.65 M=0.15, M =0.8, and l/d =10 at M =0.8 respectively. For both the l/d =1.65 cases, it is seen that the streamlines flowing over the head are deflected due to the presence of the probe. This deflection is higher for a higher Mach number. This deflection also changes the flow field near the head, distorting the sensors' readings. This deflection effect is still close to the probe body l/d =10. However, it does not affect the flow over the head; hence the probe with l/d =10 is less sensitive to the Mach number and presence of the probe body.

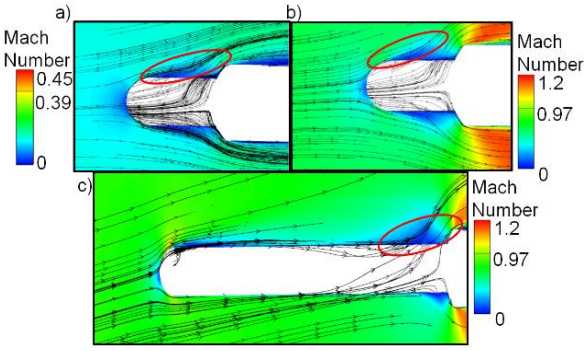

Figure 6 a) Mach contour for M=0.15, l/d= 1.65 highlighting interaction between head and probe, b) Mach contour for M=0.8, l/d= 1.65, c) Mach contour for M=0.8, l/d= 10 showing now interaction.

Figure 7 shows the coefficient value of C_{pv}, computed as Equation (1), for different values of yaw angle. The values are compared between two Mach numbers and with two different radial locations. It is seen that the C_{pv} values are smaller for higher Mach numbers. This is due to the additional energy of the flow and its ability to follow a more significant change in curvature; hence the change in pressure is lower between the yaw holes.

There is also a change in radial location. This is also attributed to a reduction in local Mach number due to the additional blockage created with the endwall and the probe body. This effect is much smaller for the l/d =10 case. There is still an effect of the Mach number, but the impact is reduced due to the decoupling of the effect of the probe body.

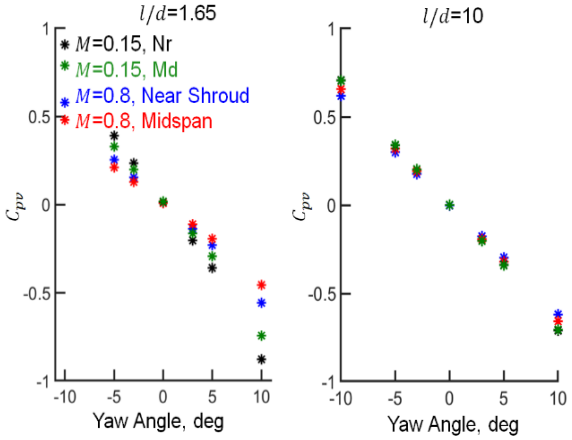

Figure 7 (left), Cpv coefficient for l/d=1.65 at four operational conditions, (right), Cpv coefficient for l/d=10.

Figure 8 shows the local isentropic Mach number at the measuring hole locations at the different operational conditions and yaw angles. The central holes are closer to the freestream Mach number for the M =0.15 case than for the M =0.8 case. Also, closer to the wall, there is a significant difference in the readings of the two pitch holes. This shows the generation of artificial pitch due to the flowfield interaction between the head and endwall, also seen in Figure 2. This difference is significantly reduced for the l/d =10 case shown in Figure 9. There is also a higher recovery of Mach number at the central holes for the l/d =10 case.

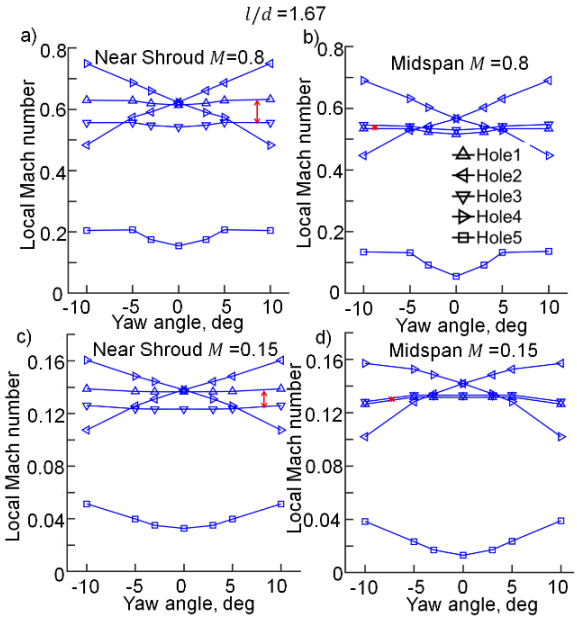

Figure 8 Local isentropic Mach number a) at freestream M=0.8, for two radial locations, b) at freestream M=0.15 at two radial locations, l/d=1.65.

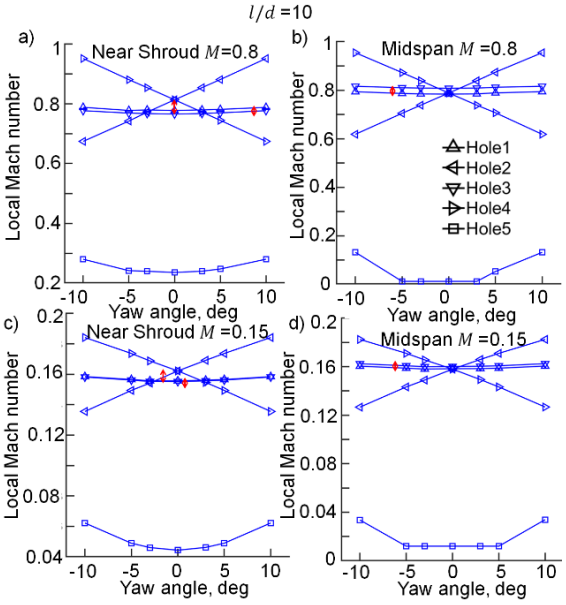

Figure 9 Local isentropic Mach number a) at freestream M=0.8 for two radial locations, b) at freestream M=0.15 at two radial locations, l/d=10.

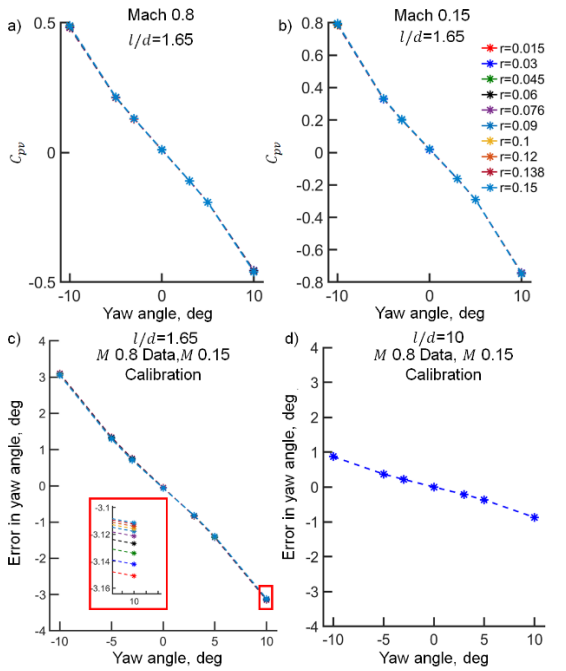

Figure 10 a) Variation of Cpv for Mach 0.8 and the effect of area of averaging, b) Variation of Cpv for Mach 0.15 and the effect of area of averaging, c) Error in angle calculation by using calibration data at M=0.15 for M=0.8 data, l/d=1.65, d) Error in angle calculation by using calibration data at M=0.15 for M=0.8 data, l/d=10.

The impact of the area of the holes is also investigated, the results shown in Figure 10 a) and b). There is no significant impact on the area of the holes. The simulations do not model the effect of the cavity of the holes; however, that is present in the real case. This is known in the literature to have an effect, as shown by Liu and Paniagua [11]. The integration of the cavity is not included in the present analysis. Figure 10 c) and d) shows the error in angle calculation due to the use of calibration coefficients obtained at 0.15, applied to data at M =0.8. We see the error increase with the yaw angle and can be as high as 3 degrees at 10-degree yaw for the l/d =1.65. The error for the l/d =10 is more minor, up to 1 degree at a 10-degree yaw.

4. BAYESIAN REGRESSION

From the results of Figure 7 we see the impact on the angle calculation due to Mach number and near wall effects. The near wall effect can also be treated as a change in Mach number case as the Mach changes near the wall. In literature, the effect of Mach has been tackled by taking calibration data at different Mach numbers and interpolating in between. However, obtaining data at different Mach numbers at test representative conditions may not always be possible. This section presents a correction methodology to evaluate the Mach number using sparse numerical data.

Due to the computational cost of numerical data, it is impossible to simulate all the combinations of angles observed in an experimental calibration. Consequently, a model is developed to fit the CFD data and provide a source of synthetic data used to generate a correction model. The procedure is shown in Figure 11.

CFD calibration data at two different conditions is taken, and a regression model is made. Gaussian Process regression is chosen to allow a better propagation and characterization of uncertainty in the model for Gaussian experimental data. A Mater3/2 kernel is used for the fits. The procedure used is described by Rasmussen [12]. The fit functions between coefficients and flow angles allow generating synthetic data that is used to map the coefficient from case 1 to the coefficient from case 2

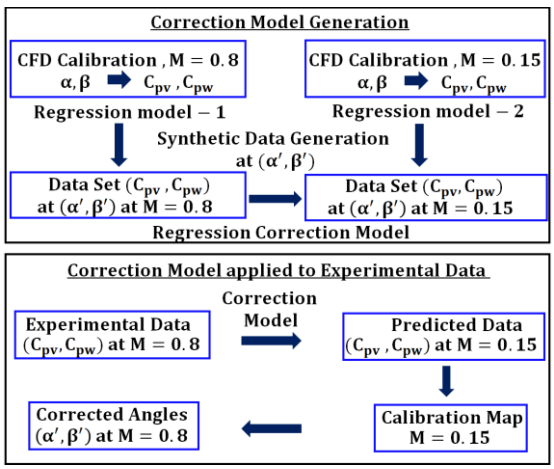

Figure 11 Procedure for Mach and wall correction

Figure 12 shows the fits and uncertainty for the coefficients for l/d =1.65 and M =0.15, and M =0.8, generated using only seven cases from CFD. Using these fit functions, 100 synthetic data points are then generated. This data is then used to create another GP regression function that corrects coefficients at M =0.8 to what they would have been, if measured at M =0.15.

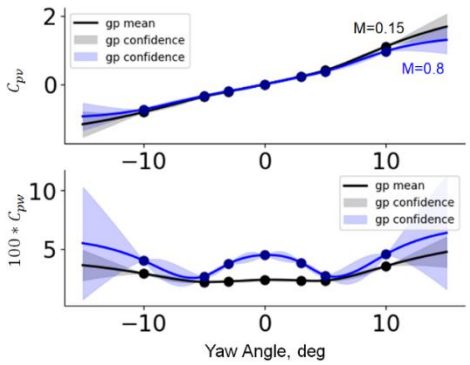

Figure 12 Gaussian Process fit for C_{pv} and C_{pw} for synthetic data generation.

Figure 13 a) shows the angle error when data at M =0.15 are used against the calibration at M =0.15 (blue) and data at M =0.8 are used against calibration at M =0.8 (red). There is a similar error level when the calibration is of the same Mach number as the data. The error increases when data at M =0.8 are used with calibration data at M =0.15 (green line). Figure 13 b) shows the comparison of the validation data at M =0.8 applied to calibration at M =0.15(blue). This data was not used for the generation of the correction function. The validation data at M =0.8, once passed through the correction function, has the same error level as the data at M =0.15 (red). This demonstrates that a correction can be provided using a small number of numerical simulations.

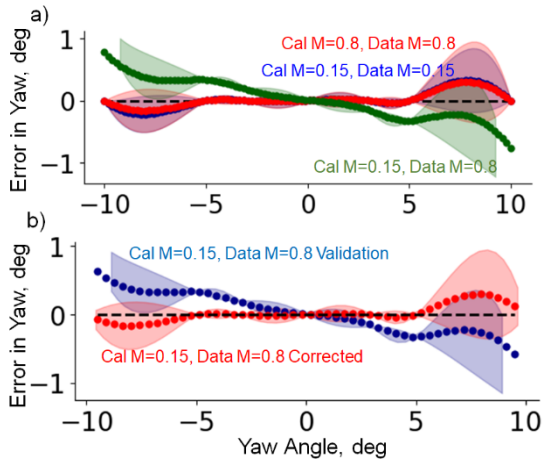

Figure 13 a) Error in angle for calibration with M=0.15 data for M=0.8 data, M=0.15 data, and M=0.8 data corrected through correction function, b) Error in angle for calibration with M=0.15 data using M=0.8 data not used for correction function generation.

5. EXPERIMENTAL DEMONSTRATION

5.1. Calibration procedure

To demonstrate the use of the correction methodology on probe data, calibration data for a five-hole probe is taken in the Purdue Experimental Turbine Aerothermal Laboratory (PETAL). Figure 14a) depicts the schematic layout of the facility, showing storage tanks capable of holding pressurized air at 150 bar, which are used to provide airflow to the desired test section [13]. The linear test section, called the Linear Experimental Aerothermal Facility, (LEAF), with a cross-sectional area of 170mm x 230mm, was used to calibrate the five-hole probes. The mass flow is measured through a calibrated critical flow Venturi upstream of the linear test section. The airflow is discharged into the test section through a fast actuation butterfly valve into the settling chamber, designed to deliver uniform conditions to the test section. The inlet Mach number is set by adjusting the mass flow. Figure 14 b) shows the LEAF facility with the side walls removed.

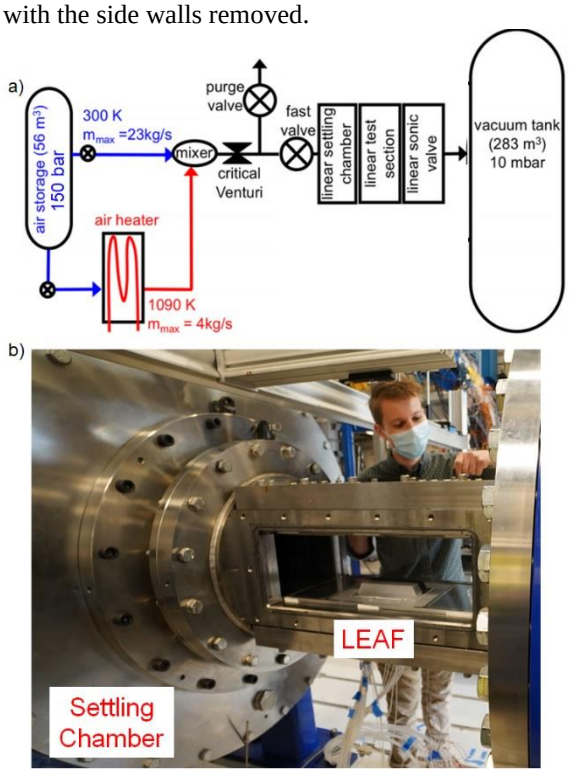

Figure 14 a) Schematic diagram of Purdue Experimental Turbine Aerothermal Laboratory, b) view of the LEAF test facility

Figure 15a) and b) show the perpendicular cone geometry of the five-hole probe head and the four-head probe rake used in this experimental calibration. As Dominy and Hodson [14] demonstrated, the perpendicular cone design allows for reduced sensitivity of the individual yaw tubes to changes in Reynolds when compared to forward-facing cone designs. Moreover, the l/d ratio of the head was set to 10 to reduce the near-wall interaction between the probe and the test section based on the

experience in the previous campaign and the results of section 3.

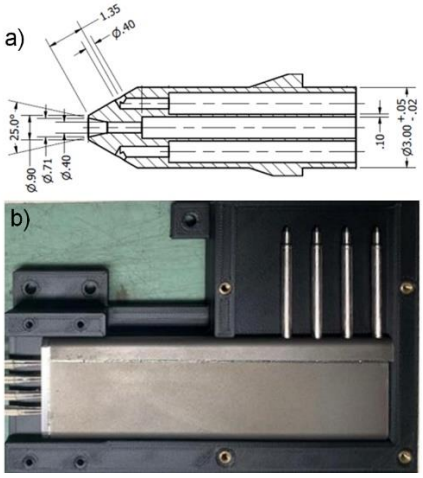

Figure 15 a) Five-Hole Probe Head Perpendicular Cone Design. b) Four-Head Five Hole Probe Rake.

The probe was calibrated at Mach 0.2 and 0.6 at different angles using an industrial KUKA KR6R700 robot with a pose repeatability of ±0.03mm. The desired Reynold's range was achievable with ambient temperature. Data was collected for a range of ±24 deg in pitch and +16deg to -24 deg in yaw at Mach 0.2 and ±12 deg in yaw at Mach 0.6. Both yaw and pitch angles were moved in steps of 4 degrees. The dynamic response of each head's pneumatic lines was assessed to determine the dwell time necessary at each traverse location. This was carried through a burst balloon test, described in [15], causing a step change in pressure. The response was recorded as the measurement returned to ambient pressure. The average time to reach 99% of the steady value was 30ms. The dwell time was set to 1s to allow a sizeable averaging window.

Before defining the traverse matrix program for the robot, it was necessary to calibrate the reference frames of the robot with respect to the linear test section to ensure the correct pitch and yaw angles are reached during the traverse and the correct initial orientation of the probe. This involved a three-step process. First, a probing stylus was connected to the robot flange, and the position of the tip with respect to the robot was calibrated using a second stylus, as shown in Figure 15 a). Second, the robot's reference frame was calibrated with respect to the reference frame of the test section by using the stylus, shown in Figure 15 b). Finally, the probe reference frame was set perpendicular to the test section reference frame using a bevel protractor, as shown in Figure 15 c). At this stage, the program was updated to reflect the positions of the measured reference frames and uploaded to the robotic arm.

Figure *17* a) illustrates the robotic arm setup mounted on the linear test section, and Figure *17* b) shows a view of the five-hole probe rake in the wind tunnel. Upstream of the probe, a total temperature thermocouple, two Kiel probes, and two static pressure taps were mounted to provide reference total pressures and to measure the inlet Mach Reynold's number.

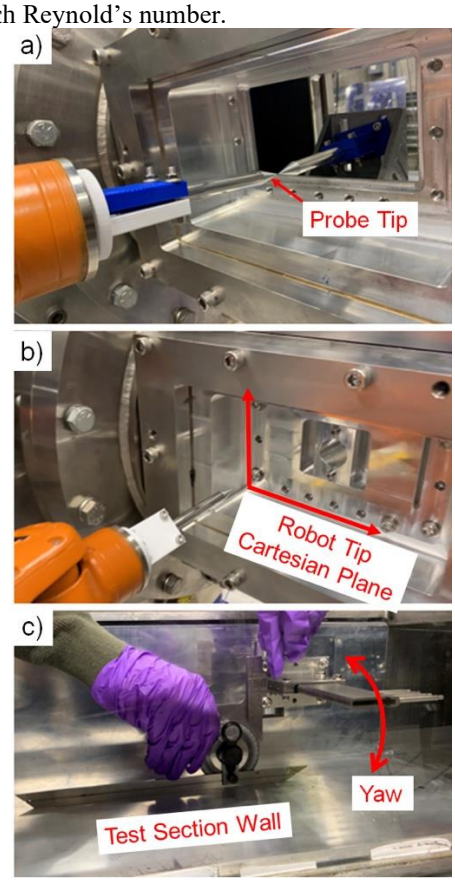

Figure 16: Calibration of the reference frame of the robot a) tip verification of the robot tip using two styli, b) robot-test section reference frame calibration using a probe and definition of reference cartesian plane, and c) validation of the probe-test section reference frames

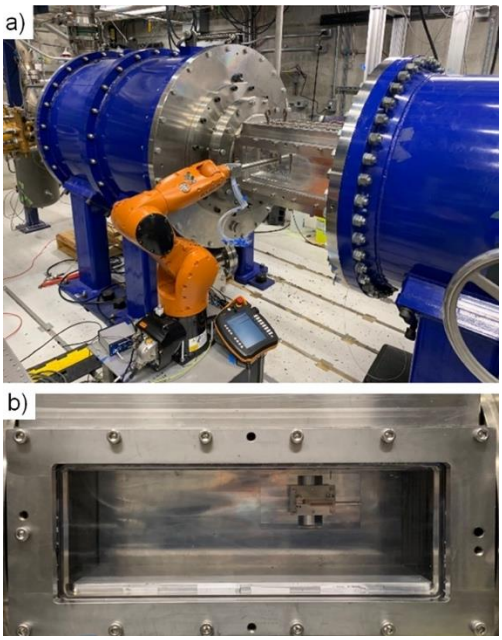

Figure 17 *a) KUKA robot integrated into the linear test section. b) five-hole probe rake in the test section.*

5.2. Correction results

The developed correction method from section 4 was used to correct data taken with the probe at two different Mach numbers, 0.2 and 0.6. Figure 18 shows the coefficients for the different Mach numbers. As can be seen, the C_{pv} coefficient values are lower on the positive side for the higher Mach number. The procedure discussed in section 5 is followed with CFD data for l/d =10. The corrected coefficients are overlaid with the experimental coefficients. It is seen that the correction does improve the matching between the two Mach numbers. The CFD analysis is carried out for symmetric heads. In practice, the actual heads are not symmetric as in the CAD due to manufacturing and assembly issues, which implies that the C_{pv} at 0-degree yaw is not close to zero. The actual experimental C_{pv} is used to correct the symmetry assumption in the correction model, and the revised coefficients are plotted in Figure 18.

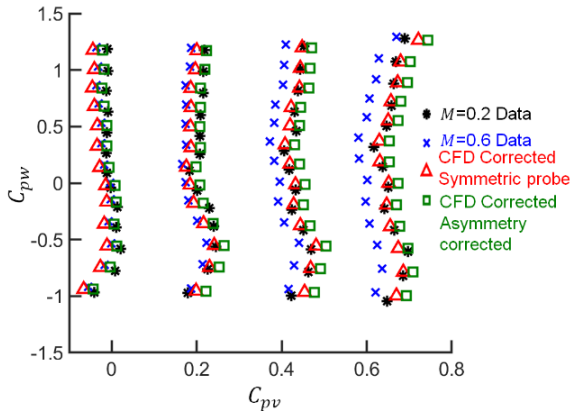

Figure 18 Cpv-Cpw plot for experimental data at M=0.2, M=0.6 and corrected Cpv-Cpw through CFD correction function.

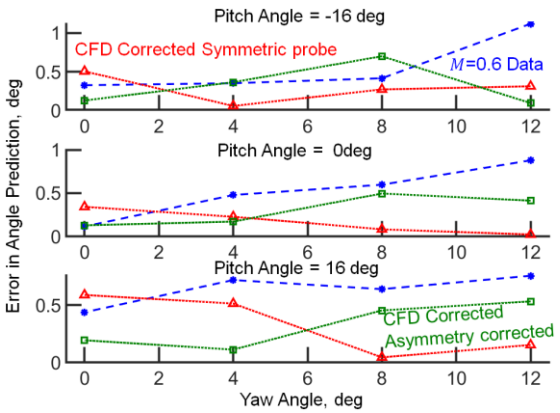

Figure 19 Error in angle from calibration at M=0.2 data and experimental data at M=0.6.

Figure 19 shows the predicted error for three different pitch angles at various yaw angles. For positive yaw angles, the error is up to 1 degree by using the M =0.2 calibration with the M =0.6 data. The corrected coefficients bring it down below 0.5 degrees but increase the error to 0 degrees due to the symmetry assumption. The asymmetry corrected coefficients decrease the error at 0 degrees and for all the other yaw angles.

CONCLUSIONS

This paper uses numerical simulations to demonstrate the effect of the Mach number and proximity to endwalls on five-hole directional probe readings. Due to the higher energy of the flow and the blockage of the stem, the local Mach number of the head, and hence the calibration coefficient, changes with the freestream Mach number and radial location of the probe. This effect can be reduced by increasing the length to diameter ratio, l/d, of the probe head. Using these results, a novel methodology is presented that uses a probabilistic Gaussian process regression model that can be used to generate a correction model for two different flow conditions. Using this model, data collected at a given Mach number can be used with calibration data collected at a different Mach number. Experimental calibration data is collected at two different Mach numbers at M=0.2 and 0.6. The correction methodology is then used to correct the coefficient from M=0.6 data to M=0.2 data. The error in angle calculation decreases from 1 degree at a 12-degree yaw to less than 0.1 degrees with the correction. This demonstrates the viability of using sparse numerical data to correct the experimental Mach number effect.

REFERENCES

[1] P. Gaetani and G. Persico, "Technology Development of Fast-Response Aerodynamic Pressure Probes," International Journal of Turbomachinery, Propulsion and Power, vol. 5, no. 2, p. 6, Apr. 2020, doi: 10.3390/ijtpp5020006.

[2] P. D. Smout and P. C. Ivey, "Investigation of Wedge Probe Wall Proximity Effects: Part 1—Experimental Study," *Journal of Engineering for Gas Turbines and Power*, vol. 119, no. 3.

[3] P. D. Smout and P. C. Ivey, "Investigation of Wedge Probe Wall Proximity Effects: Part 2—Numerical and Analytical Modeling," *Journal of Engineering for Gas Turbines and Power*, vol. 119, no. 3, pp. 605–611, Jul. 1997, doi: 10.1115/1.2817027.

[4] K. M. Argüelles Di´az, J. M. Ferna´ndez Oro, E. Blanco Marigorta, and R. Barrio Perotti, "A Numerical 3-D Model of a Trapezoidal Three-Hole Pneumatic Pressure Probe for Incompressible Flow." Proceedings of the ASME 2010 3rd Joint US-European Fluids Engineering Summer Meeting collocated with 8th International Conference on Nanochannels, Microchannels, and Minichannels. ASME 2010 3rd Joint US-European Fluids Engineering Summer Meeting: Volume 2, Fora. Montreal, Quebec, Canada. August 1–5, 2010. pp. 159-167. ASME. https://doi.org/10.1115/FEDSM-ICNMM2010-30713 .

[5] D. Delhaye, G. Paniagua, J. M. F. Oro, and R. Denos, Enhanced performance of fast-response 3-hole wedge probes for transonic flows in axial turbomachinery. Exp Fluids 50, 163–177 (2011). https://doi.org/10.1007/s00348-010-0908-y .

[6] L. Bhatnagar *et al.*, "Uncertainty in High-Pressure Stator Performance Measurement in an Annular Cascade at Engine-Representative Reynolds and Mach," *Journal of Engineering for Gas Turbines and Power*, vol. 144, no. 2, p. 021001, Feb. 2022, doi: 10.1115/1.4052385.

[7] A. L. Treaster and A. M. Yocum, "The Calibration and Application of Five Hole Probes." NAVSEA Technical Memorandum File, TM 78-10, Jan. 18, 1978 .

[8] A. J. Pisasale and N. A. Ahmed, "Theoretical calibration for highly three-dimensional low-speed flows of a five-hole probe," *Meas. Sci. Technol.*, vol. 13, no. 7, pp. 1100–1107, Jul. 2002, doi: 10.1088/0957-0233/13/7/318.

[9] T. Yasa and G. Paniagua, "Robust procedure for multi-hole probe data processing," *Flow Measurement and Instrumentation*, vol. 26, pp. 46–54, Aug. 2012, doi: 10.1016/j.flowmeasinst.2012.03.004.

[10] C. Sieverding, L. Maretto, F. Lehthaus, O. Lawaczeck, and D.-A. Göttingen, "Design and Calibration of Four Probes for use in the Transonic Cascade Testing", Von Karman Institute for Fluid Dynamics Technical Note 100, p. 61, 1974 .

[11] Z. Liu and G. Paniagua, "Design of Directional Probes for High-Frequency Turbine Measurements," *Journal of Engineering for Gas Turbines and Power*, vol. 140, no. 1, p. 011601, Jan. 2018, doi: 10.1115/1.4037640.

[12] C. E. Rasmussen and C. K. I. Williams, *Gaussian processes for Machine learning*. Cambridge, Mass: MIT Press, 2006.

[13] G. Paniagua *et al.*, "Design of the Purdue Experimental Turbine Aerothermal Laboratory for Optical and Surface Aerothermal Measurements," *Journal of Engineering for Gas Turbines and Power*, vol. 141, no. 1, p. 012601, Jan. 2019, doi: 10.1115/1.4040683.

[14] R. G. Dominy and H. P. Hodson, "An Investigation of Factors Influencing the Calibration of 5-Hole Probes for 3-D Flow Measurements." Proceedings of the ASME 1992 International Gas Turbine and Aeroengine Congress and Exposition. Volume 1: Turbomachinery. Cologne, Germany. June 1–4, 1992. V001T01A077. ASME. https://doi.org/10.1115/92-GT-216 .

[15] G. Paniagua and R. Dénos, "Digital compensation of pressure sensors in the time domain," *Experiments in Fluids*, vol. 32, no. 4, pp. 417–424, Apr. 2002, doi: 10.1007/s003480100355.